

# Footprints of the QCD Crossover on Cosmological Gravitational Waves at Pulsar Timing Arrays

Gabriele Franciolini,<sup>1,\*</sup> Davide Racco,<sup>2,†</sup> and Fabrizio Rompineve<sup>3,4,5,‡</sup>

<sup>1</sup>*Dipartimento di Fisica, Sapienza Università di Roma and INFN, Sezione di Roma, Piazzale Aldo Moro 5, 00185, Rome, Italy*

<sup>2</sup>*Stanford Institute for Theoretical Physics, Stanford University, 382 Via Pueblo Mall, Stanford, CA 94305, U.S.A.*

<sup>3</sup>*CERN, Theoretical Physics Department, Esplanade des Particules 1, Geneva 1211, Switzerland*

<sup>4</sup>*Departament de Física, Universitat Autònoma de Barcelona, 08193 Bellaterra, Barcelona, Spain*

<sup>5</sup>*Institut de Física d'Altes Energies (IFAE) and The Barcelona Institute of Science and Technology (BIST), Campus UAB, 08193 Bellaterra (Barcelona), Spain*

Pulsar Timing Arrays (PTAs) have reported evidence for a stochastic gravitational wave (GW) background at nHz frequencies, possibly originating in the early Universe. We show that the spectral shape of the low-frequency (causality) tail of GW signals sourced at temperatures around  $T \gtrsim 1$  GeV is distinctively affected by confinement of strong interactions (QCD), due to the corresponding sharp decrease in the number of relativistic species. A Bayesian analysis in the latest International PTA dataset reveals a significant improvement in the fit with respect to cubic power law spectra, previously employed for the causality tail. Comparison with the results of NANOGrav 15 years and European PTA Data Release 2 suggests that our inclusion of Standard Model effects on GWs can have a potentially decisive impact on model selection.

## I. Introduction

A stochastic background of Gravitational Waves (SGWB) may be the only direct probe into the elusive early (pre-recombination) stages of cosmological evolution, where it can be produced in the presence of physics beyond the Standard Model (SM). Not surprisingly, the recently-reported evidence for a nHz SGWB in the NANOGrav 15 years [1, 2] (NG15), European Pulsar Timing Array Data Release 2 (EPTA-DR2) [3, 4], Parkes [5, 6] and Chinese [7] PTAs datasets, whose uncorrelated component was already detected with previous data [8–11], has attracted ample attention in the astrophysics, cosmology and particle physics communities.

At this stage, one of the most urgent endeavors is determining whether the observed signal is of cosmological or astrophysical origin, in the latter case sourced by supermassive black hole binaries (SMBHBs), see e.g. [12, 13] for an overview. This task is challenging for multiple reasons. First, while the NG15 analysis suggests that the astrophysical model may face challenges [14], the current understanding of SMBHBs is not sufficiently precise to draw conclusions (see the predictions reported by EPTA-DR2 [15], as well as e.g. [11, 16]); Second, the spectral shape of a cosmological SGWB generically depends on the microphysical nature of the source and often has to be extracted by means of case-by-case numerical simulations.

In this Letter, we show that a distinctive signature is nonetheless imprinted model-independently by the early-Universe dynamics of the SM, in the GW spectra of a broad class of early Universe sources. These are often referred to as causality-limited, i.e. radiating GWs at a definite epoch in the cosmological history, on time scales comparable to or smaller than the corresponding Hubble time. Examples of such sources are: first order phase transitions (PTs) [17], annihilation of cosmic domain walls [18], collapse of large density perturbations [19] (see [15, 20–26] for searches in and [27–31] for interpretations of PTA data), and arise in several well-motivated beyond the SM (BSM) scenarios (see instead [15, 26, 32–35] for PTA-related analyses of other types of possible cosmological SGWBs).

Our starting point is a fortuitous coincidence of scales: the nHz frequencies probed by PTAs coincide with those of GWs that re-enter the Hubble horizon at the epoch of the QCD crossover phase transition in the hot Universe, i.e. at temperatures  $T \sim 100$  MeV (see e.g. [36]). While the crossover itself is not expected to source GWs, the rapid drop in the number of relativistic degrees of freedom in the thermal bath (due to the formation of hadrons) causes a significant change in the equation of state (EoS) of the Universe, that is precisely determined by means of lattice QCD calculations [37].

In the presence of a causality-limited GW source that is active at temperatures higher than the QCD crossover, such a change in the EoS affects the low-frequency tail of the GW signal, which we refer to as Causality Tail (CT), whose properties are largely independent of the specific source. The spectral shape of the CT is altered due to both the redshift of the SM radiation bath (previously pointed out for different types of GW signals, e.g. [38,

\* gabriele.franciolini@uniroma1.it

† dracco@stanford.edu

‡ fabrizio.rompineve@cern.ch

39]) as well as the different evolution of sub- and super-horizon GW modes (e.g. [40–42]).

This Letter derives in detail the spectral shape of CT signals at nHz frequencies, that can be readily used by PTA collaborations, GW and BSM communities for model comparison (improving upon simple power-law CTs, currently adopted by NG15 [26] and EPTA-DR2 [15], see also [21, 22]) using present and future datasets. Importantly, we show that that our novel inclusion of QCD-induced features significantly impacts the interpretation of current PTA data, by performing a Bayesian search for a CT signal in the International PTA data release 2 (IPTA-DR2) dataset [11, 43], and by comparing with the latest results from NG15 and EPTA-DR2.

## II. Standard Model features in the causality tail of primordial GW backgrounds

Focusing on cosmological SGWBs, a powerful property is ensured in a broad class of primordial sources where GWs are generated locally, independently in each spatial patch, and in a limited amount of time. The correlation length  $\ell_*$  of the source of GWs must then be finite, and causality guarantees that  $\ell_* < H^{-1}(t)$  at the time when emission shuts off, where  $H$  is the Hubble expansion rate. We denote by  $f_{\text{CT}}$  the frequency of the GW mode crossing the Hubble radius at that time. The remarkable property of the *causality tail* (CT) is that all GW frequencies  $f < f_{\text{CT}}$  evolve independently of the source, because the corresponding wavelengths are  $f^{-1} > \ell_*$ . The evolution of each tensor mode  $h_k(t)$  in this regime is sensitive only to the expansion of the Universe and GW propagation effects [38, 44–72]. A prototypical example is the case of cosmological PTs, see e.g. [55, 63, 73, 74]. In this case, both bubble collisions and sound waves (and possibly plasma turbulence) can act as causality-limited sources, each with its own finite correlation length.

The GW energy fraction is customarily defined as

$$\Omega_{\text{GW}}(f) \equiv \frac{1}{\rho_{\text{cr}}} \frac{d\rho_{\text{GW}}(f)}{d \ln f} \quad (1)$$

where  $\rho_{\text{cr}}$  is the critical energy density today.  $\Omega_{\text{GW}}(f)$  exhibits a spectral shape, that is typically peaked at some frequency  $f_* > f_{\text{CT}}$ . The CT of the spectrum ( $f \lesssim f_{\text{CT}}$ ) is well-known to behave as  $\Omega_{\text{GW}}(f) \propto f^3$  in a universe filled by a perfect relativistic fluid with EoS  $w(t) = p/\rho = \frac{1}{3}$ , see e.g. [55]. This tilt can be modified by two effects:

1. The GW energy density  $\rho_{\text{GW}}(f)$  in the CT is determined by the expansion history of the Universe and the GW propagation after generation [40];
2. The critical energy density  $\rho_{\text{cr}} = \rho_{\gamma,0}/\Omega_{\gamma,0}$  in Eq. (1), where  $\Omega_{\gamma,0}h^2 = 2.47 \times 10^{-5}$  is the SM radiation abundance today,  $h \equiv H_0/(100 \text{ km/s/Mpc})$  and  $H_0$  is the Hubble expansion rate today, is affected

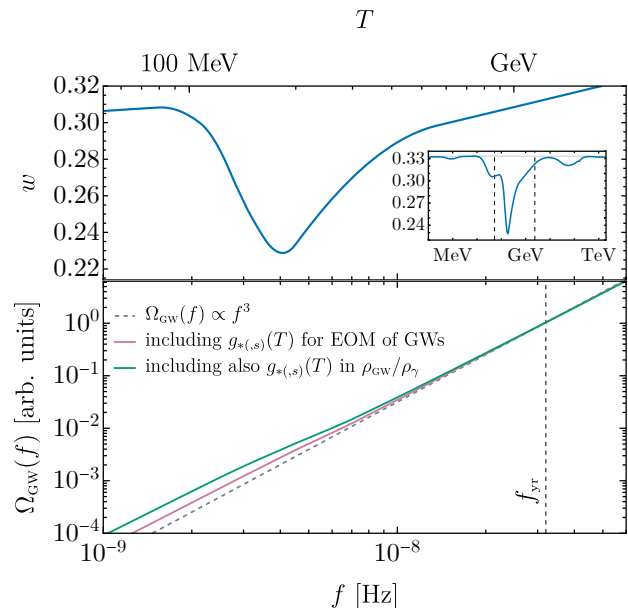


FIG. 1. *Top*: Variation of the EoS with the temperature of the Universe during the QCD crossover. The inset shows  $w$  in an expanded range. *Bottom*: Impact of the variation of  $w(T)$ ,  $g_*(T)$  during the QCD crossover on the low frequency tail of a causality-limited primordial SGWB (here plotted with an arbitrary amplitude). The dashed line shows the  $f^3$  scaling obtained in a pure radiation-dominated universe.

by entropy injections originating e.g. from freeze-out processes occurring for SM (or BSM) particles in the thermal bath [38].

The first effect comes from the evolution of super-Hubble tensor modes [40]. After the GW source shuts off, the emitted super-Hubble modes freeze due to Hubble friction, remain practically constant until horizon re-entry, and then proceed with under-damped oscillations diluted as  $1/a$ . As a result, the CT scales as

$$\left. \frac{d\rho_{\text{GW}}(f)}{d \ln f} \right|_{f < f_{\text{CT}}} \propto f^{3+2\frac{3w-1}{3w+1}}, \quad (2)$$

for a generic  $w$ . This scaling can be additionally affected by relativistic free-streaming particles, as we discuss further below.

The second effect on the other hand concerns only the SM radiation bath, since GWs are decoupled and do not receive entropy injections from other species (analogously to neutrinos at the epoch of electron-positron annihilation). Therefore, this leads to a temperature-dependent modulation

$$\Omega_{\gamma}(T) = \Omega_{\gamma,0} \left( \frac{g_{*,s}(T_0)}{g_{*,s}(T)} \right)^{4/3} \left( \frac{g_*(T)}{g_*(T_0)} \right) \left( \frac{a_0}{a} \right)^4, \quad (3)$$

$g_*(T) = \rho/(\pi^2 T^4/30)$  and  $g_{*,s}(T) = s/(2\pi^2 T^3/45)$  being the effective number of degrees of freedom in energy ( $\rho$ ) and entropy ( $s$ ) densities respectively, and  $a(a_0)$  is the

scale factor (today). From the thermodynamical relation  $sT = p + \rho$  one infers the temperature-dependent EoS :  $w(T) = \frac{4}{3}(g_{*,s}(T)/g_*(T)) - 1$ .

During the QCD crossover, heavy hadrons form and both  $g_{*,s}(T)$  and  $g_*(T)$  decrease rapidly with temperature. Their values and the EoS (shown in the upper plot of Fig. 1) are precisely determined with lattice QCD techniques [37]. The temporary decrease of  $w(T)$  is due to the pressureless contribution of QCD matter to the thermal bath, followed by its rapid depletion. Therefore, the CT is distinctively modified, when the corresponding GW modes with wavenumber  $k$  re-enter the Hubble horizon during the QCD crossover. Their frequency is set by  $f = k/2\pi = aH/2\pi$ , which in terms of temperatures reads (see App. A)

$$f \simeq 3.0 \text{ nHz} \cdot \left( \frac{g_{*,s}(T)}{20} \right)^{1/6} \left( \frac{T}{150 \text{ MeV}} \right). \quad (4)$$

We solve the equations of motion for  $h_k(t)$  (see e.g. [40], and App. B for details), accounting for the temperature dependence of  $w$  and  $g_*$  and obtain the spectrum shown in Fig. 1 (lower plot, solid green curve). A clear deviation from the commonly employed  $f^3$  approximation can be appreciated, accidentally located in the nHz range where PTA experiments are most sensitive to SGWBs.

Beyond the SM effects presented above, we notice that a CT signal probes the cosmic expansion history back to  $T_{\text{QCD}}$ . In particular, the possible presence of a fraction  $f_{\text{FS}} \equiv \rho_{\text{FS}}/\rho_{\text{tot}}$  of free-streaming species is easily accounted for, by multiplying the  $\Omega_{\text{CGW}}$  spectrum shown in Fig. 1 by  $f^{16f_{\text{FS}}/5}$ , for  $f_{\text{FS}} \lesssim 15\%$  [40].

### III. GW backgrounds at Pulsar Timing Arrays

A SGWB can be described in terms of the characteristic strain  $h_c(f) \simeq 1.26 \cdot 10^{-9} \cdot (\text{nHz}/f) \sqrt{\Omega_{\text{CGW}}(f) h^2}$  [55]. This induces the cross-power spectral density for the timing residuals  $S_{ab}(f) = \Gamma_{ab} h_c^2(f) / (12\pi^2 f^3)$ , where  $\Gamma_{ab}$  contains correlation coefficients between pulsars  $a$  and  $b$  and is given by the Hellings-Downs function [75] for a SGWB. PTA collaborations typically assume a power-law shape  $h_c(f) = A_{\text{CP}}(f/f_{\text{yr}})^\alpha$  for the characteristic strain (or  $S_{ab}(f) \propto (f/f_{\text{yr}})^{-\gamma}$  with  $\gamma = 3 - 2\alpha$ ), so that the corresponding GW fraction is

$$\Omega_{\text{CGW}}(f) h^2 \simeq 6.3 \cdot 10^{-10} \left( \frac{A_{\text{CGW}}}{10^{-15}} \right)^2 \left( \frac{f}{f_{\text{yr}}} \right)^{n_T} \quad (5)$$

where  $f_{\text{yr}} \equiv (1 \text{ yr})^{-1} \simeq 32 \text{ nHz}$  and  $n_T = 2(\alpha + 1) = 5 - \gamma$ . For a cosmological SGWB, we use the subscript CGW rather than CP. While an astrophysical SGWB from SMBHBs is expected, its properties are not yet fully understood. In particular, population synthesis studies suggest a wide possible range for the amplitude and  $\alpha$ , see e.g. [11, 12, 15, 16, 26, 76–80]. The simple prediction

$\alpha = -\frac{2}{3}$  is instead valid only if the orbits are circular and energy loss is dominated by gravitational radiation [81]. This corresponds to a slope  $n_T = \frac{2}{3}$  for  $\Omega_{\text{CGW}}(f)$  (and  $\gamma = \frac{13}{3}$ ).

On the other hand, a power-law approximation with  $n_T = 3$  (i.e.  $\alpha = \frac{1}{2}, \gamma = 2$ ) is assumed in the literature when modeling the causality tail (CT) of a CGW.<sup>1</sup> The main novelty of our work is that the actual shape of such a CT exhibits relevant deviations from a simple power law, when  $f_{\text{CT}}$  lies above the frequency bins employed in PTA analyses, i.e.  $10 \text{ nHz} \lesssim f_{\text{CT}} \lesssim f_*$ . A convenient parametrization for the characteristic strain of the CT is

$$h_{\text{c,CT}}(f) = A_{\text{CT}} \frac{\mathcal{S}(f)}{\mathcal{S}(f_{\text{CT}})} \left( \frac{f_{\text{CT}}}{f} \right)^{-\frac{8}{5} f_{\text{FS}}}, \quad (6)$$

where  $\mathcal{S}(f)$  is tabulated in App. B and normalised to  $\mathcal{S}(f_{\text{yr}}) = 1$ , while  $A_{\text{CT}}$  is the amplitude at  $f_{\text{CT}}$ . Fig. 1 shows  $\Omega_{\text{CGW}}(f) \propto f^2 \mathcal{S}^2(f)$  (i.e. with  $f_{\text{FS}} = 0$ ).

A second crucial difference between astrophysical and CGW backgrounds is that *only* the latter contribute to energy budget of the Universe at early times, and can affect cosmological observables if they are present in a significant quantity, as any other relativistic free-streaming component beyond the SM. In other words, a CGW contributes to the *effective number of neutrino species* as  $N_{\text{eff}} \equiv 3.044 + \Delta N_{\text{eff}}^{\text{CGW}}$ , with  $\Delta N_{\text{eff}}^{\text{CGW}} = \rho_{\text{CGW}}/\rho_{\nu,1}$  and  $\rho_{\nu,1}$  is the energy density of a single neutrino species. The latest measurements of the Cosmic Microwave Background (CMB) anisotropies and Baryon Acoustic Oscillations (BAO) impose  $\Delta N_{\text{eff}} \leq 0.28$  at 95% C.L. [82]. This constrains the CGW relic abundance to (e.g. [55])  $\Omega_{\text{CGW}} h^2 \simeq 1.6 \cdot 10^{-6} (\Delta N_{\text{eff}}^{\text{CGW}}/0.28)$ , where  $\Omega_{\text{CGW}}$  is the total (integrated) relic abundance. A model-independent bound then applies to any search for CGWs. For the peaked sources of our interest,  $\Omega_{\text{CGW}} \simeq \Omega_{\text{CGW}}(f_*)$  and the constraint translates to

$$A_{\text{CGW}} \leq 5 \times 10^{-14} \left( \frac{f_{\text{yr}}}{f_*} \right)^{1+\alpha}, \quad (95\% \text{ C.L.}), \quad (7)$$

for signals that can be approximated with power-laws up to  $f_*$ . While this assumption is often not valid (see e.g. [83, 84] for the case of PTs), the  $\Delta N_{\text{eff}}^{\text{CGW}}$  bound can be applied model-independently to the CT of the signal, thereby giving  $A_{\text{CT}} \leq 5 \times 10^{-14} (f_{\text{yr}}/f_{\text{CT}})$ . This often captures the approximate strength of the constraint, since typically  $f_{\text{CT}} \lesssim (0.1 - 1)f_*$  and the spectrum flattens close to the peak. By comparison with Eq. (5), it is evident that CMB constraints can affect signal interpretation when  $f_* \gtrsim f_{\text{yr}}$ , if  $\alpha \geq -1$  (see also [85]).

Finally, let us remark that GWs with frequency  $f \gtrsim f_{\text{CT}}$  provide an unavoidable contribution to  $f_{\text{FS}} \sim 0.3 \Delta N_{\text{eff}}^{\text{CGW}}$ , see also App. B.

<sup>1</sup> The high-frequency tail  $f \gtrsim f_*$  may also be a power law in the PTA band, when  $f_* \lesssim \text{nHz}$ . However, unlike the CT, its shape is model-dependent and disfavored by latest PTA results [2, 4, 6].

#### IV. Bayesian Analysis and Comparison with Latest Datasets

We now present the results of a Bayesian search for the CT of a CGW signal in the IPTA-DR2 [11] dataset. Our aim is to quantify the impact of the QCD-induced deviations from a power law with  $n_T = 3$  on PTA signal interpretation. We discuss the implications for the NG15 and EPTA-DR2 results further below. Following the IPTA collaboration [11], we limit our analysis to the first 13 frequency bins of the dataset, to avoid pulsar-intrinsic excess noise at high frequencies. Additionally, we consider only auto-correlation terms, rather than the full HD function, as in [11].

We consider two CGW models: the CT and the single power law  $n_T = 3$ , both with only one free parameter,  $A_{\text{CT}}$  and  $A_{\text{CGW}}$  respectively. We impose the  $\Delta N_{\text{eff}}$  constraints in (below) Eq. (7) to  $A_{\text{CGW}}$  ( $A_{\text{CT}}$ ). For the CT signal, we fix  $f_{\text{FS}}$  to the unavoidable contribution from GWs of frequency  $f = f_{\text{CT}}$  (see App. B for details). We set  $f_{\text{CT}} = f_{\text{yr}}$  (such that the first bins of both datasets are guaranteed to be deep in the CT) and similarly  $f_* = f_{\text{yr}}$  for the  $n_T = 3$  model, and comment on other choices below. Additionally, we compare with common power-law processes (non-CGW) with free exponent  $\gamma$ , as well as with  $\gamma = \frac{13}{3}$  (i.e.  $n_T = \frac{2}{3}, \alpha = -\frac{2}{3}$ ). App. E lists all parameters and prior choices.

We compare models by computing the Bayes factors  $\mathcal{B}_{ij}$ , quantifying the preference of model  $i$  with respect to model  $j$ . These are reported in Tab. I.

$\mathcal{M}_1 \backslash \mathcal{M}_2$	Causality Tail	Free $n_T$	$n_T = \frac{2}{3}$ ( $\gamma = \frac{13}{3}$ )
$f^3$	<b>1.3</b>	3.2	4.0
Causality Tail	—	1.8	2.7

TABLE I.  $\log_{10} \mathcal{B}_{\mathcal{M}_1, \mathcal{M}_2}$  for the models considered in this work, based on the IPTA-DR2 dataset. Notice that the ‘‘Causality Tail’’ (CT) spectrum (shown in Fig. 1), which deviates from  $f^3$  due to the cosmological history around the QCD crossover, is *strongly* preferred with the respect to the  $f^3$  spectrum. The  $\Delta N_{\text{eff}}$  upper bound on cosmological SGWB has been imposed on the amplitude of CT and  $f^3$  spectra, fixing  $f_{\text{CT}} = f_{\text{yr}}$  for the CT and  $f_* = f_{\text{yr}}$  for  $n_T = 3$ .

One important result is the comparison between CT and the power-law  $n_T = 3$  signals. As highlighted in bold in Tab. I, the CT provides a better fit than  $f^3$  to the IPTA-DR2 dataset, with a Bayes factor that indicates ‘‘strong evidence’’ for CT over  $f^3$ .

In the same dataset, the astrophysical signal modeled with a free power law is preferred over the CT signal with a similar Bayes factor, whereas the evidence over the  $n_T = 3$  signal is decisive. These Bayes factors further increase when comparing to a fixed power-law signal with  $\gamma = \frac{13}{3}$ . The GW spectra and corresponding CP time delays for maximum-likelihood values of parameters obtained by our analyses are shown in Fig. 2. Both plots

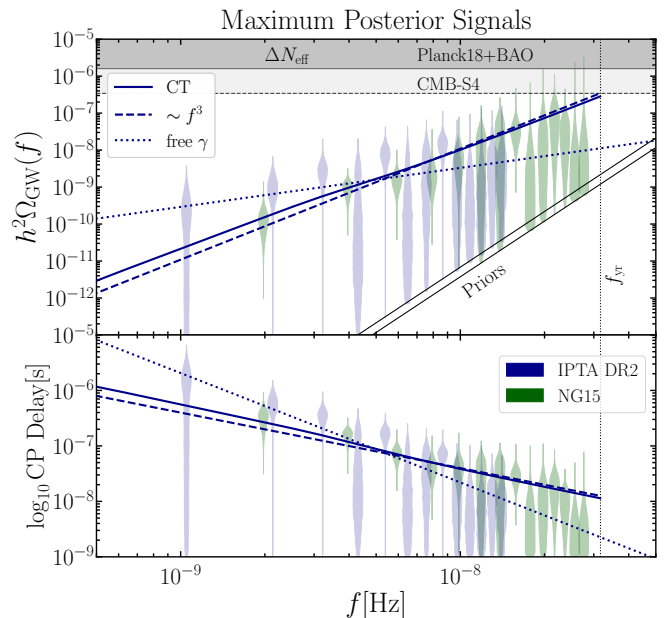


FIG. 2. We compare the CT (solid),  $n_T = 3$  (dashed) and astrophysical free  $\gamma$  (dotted) models, plotted both in terms of the GW relic spectrum (*upper*) and the induced CP time delays  $\sqrt{S_{ab}(f)}/T$ ,  $T$  being the observation time of the PTA (*lower*), for maximum posterior values of parameters obtained by a Bayesian analysis in the IPTA-DR2 dataset. In the upper panel, the gray-shaded region shows the CMB+BAO upper bound on  $\Delta N_{\text{eff}}$ , and the dotted line is the detection reach for CMB-S4 experiments. The violin posteriors in the upper plot are obtained by adapting the results of IPTA-DR2 [11] (blue) and NG15 [2] (green), shown in the lower panel. The lower limits of these posteriors are determined by the prior choice of [2, 11]; the corresponding region is marked by a black line in the lower right corner of the upper panel for clarity. See App. E for parameter posteriors.

clearly show why the CT presented in our work improves the fit to PTA data, when compared to the  $n_T = 3$  power law: for  $A_{\text{CT}} = A_{\text{CGW}}$  the CT allows for a larger amplitude of  $\Omega_{\text{GW}}$  and of CP delays in the first bins (roughly by a factor of 2 – 3). The difference in Bayes factors is also partially due to the fact that the  $n_T = 3$  signal lies significantly out of the preferred ( $3\sigma$ ) region of parameter space [11], see Fig. 3.

The curve in Fig. 2 corresponds to a negligible value of  $f_{\text{FS}}$  from GWs of frequency  $f = f_{\text{CT}}$ . Additional contributions from higher frequencies and/or other free-streaming species are model-dependent, but would affect our results only if  $\Delta N_{\text{eff}}^{\text{CGW}} \gtrsim 0.1$ . Interestingly, in this case an excess in upcoming cosmological surveys [86–88] is expected.

Our Bayesian analysis relies on the data, timing and noise model used by the IPTA-DR2 collaboration. These have been improved in most recent PTA data releases and it is thus natural to ask how the comparison between the realistic CT signal presented in our work and other models is affected. While a complete assessment

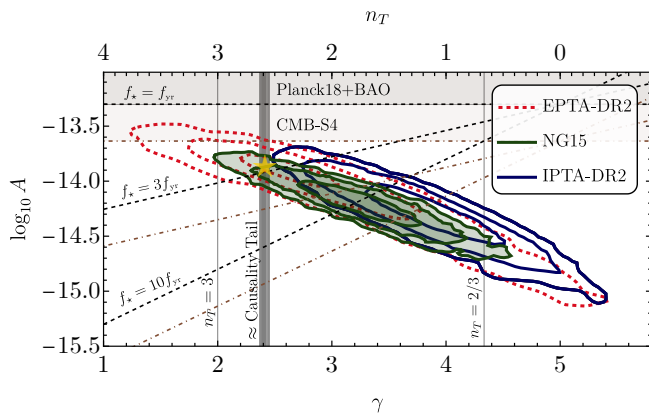


FIG. 3. Posteriors for a common process power-law model from IPTA-DR2 [11] (blue), NG15 (green, shaded) and EPTA-DR2 (red, dotted), the last two enforcing HD correlations in the analyses [2, 4]. The vertical lines highlight the tilts discussed in the text, approximately describing to a CT signal. We also show current and future  $\Delta N_{\text{eff}}$  bounds that affect any power-law signal extending up to  $f_{\star} = 1, 3, 10 f_{\text{yr}}$ . The yellow star indicate the best fit amplitude for the CT model obtained with a simplified fit of the NG15 results.

requires a Bayesian search in the new datasets, it is possible to draw some conclusions by looking at the posterior distributions for the power-law parameters  $\gamma$ ,  $A$  presented by NG15 [2] and EPTA-DR2 [15] (we use the DR2new HD results) and reported in Fig. 3. Both results significantly overlap with the posteriors of IPTA-DR2 (notice that the new posteriors are obtained including HD correlations). Furthermore, the NG15 and EPTA-DR2 ( $2\sigma$ ) posteriors are shifted to smaller values of  $\gamma$ , i.e. larger  $n_T$ . This has the following implication: the  $n_T = \frac{2}{3}$  ( $\gamma = \frac{13}{3}$ ) slope is now beyond the preferred  $2\sigma$  region of both posteriors, therefore the evidence for this tilt over  $n_T = 3$  is expected to drop significantly with respect to the Bayes factor reported in Tab. I.

Very interestingly, a simplified analysis of the CT signal suggests that it should be significantly favoured with respect to both the  $n_T = 3$  and  $n_T = \frac{2}{3}$  models in the new datasets. Indeed, while the CT in general cannot be approximated by a power law over the full range of frequencies of the recent PTA datasets, one can understand its approximate behavior by evaluating the slope of the signal through a given number of frequency bins. The result of this procedure is shown by the vertical gray lines in Fig. 3, which have been obtained by fitting the CT with a power law through the lowest 4th to 8th frequency bins of the NG15 dataset, where evidence for GWs is reported (and within the 9 frequency bins employed by EPTA-DR2). We also perform a simplified log-likelihood analysis of the NG15 data, fitting the free spectrum posterior distributions for the 14 frequency bins reported in Ref. [2]. We show the corresponding best fit amplitude with a marker in Fig. 3. We thus expect the CT to provide as good a fit to the NG15 (EPTA-

DR2) data as a power-law model with parameters inside the  $2\sigma$  ( $1\sigma$ ) region of the posteriors. The free spectrum posteriors from [2] are also reported in Fig. 2 (green), showing that the maximum posterior signals from the IPTA-DR2 analysis should also provide good fits to the NG15 data.

Finally, let us comment on how a different choice for  $f_{\text{CT}}$  affects our model comparison. If  $f_{\text{CT}} > f_{\text{yr}}$ , the  $\Delta N_{\text{eff}}$  bound on  $A_{\text{CT}}$ ,  $c_{\text{GW}}$  forces the CGW to be lower, especially if its tilt is steeper. The CMB constraint on power-law CGWs is shown in Fig. 3 for any tilt, for several choices of cutoff (or peak) frequency  $f_{\star} = f_{\text{yr}}$  (shaded region),  $3f_{\text{yr}}, 10f_{\text{yr}}$  (region above dashed tilted lines). The reach of CMB-S4 [88] surveys is also plotted with dot-dashed brown curves, interestingly probing a part of the preferred EPTA-DR2 region. As expected from Fig. 3, in our search we find that the 13-bins IPTA-DR2 dataset decisively disfavors a CT extending above  $\sim 32$  nHz. For the latest PTA datasets, the  $\Delta N_{\text{eff}}$  bound constrains the  $3\sigma$  results only if  $f_{\text{CT}} \gtrsim 50$  nHz and completely excludes the CT signal only if  $f_{\text{CT}} \gtrsim 100$  nHz.

## V. Discussion and Implication for Particle Physics

We have pointed out that SM physics predicts a specific shape for the CT of a GW signal, that can be clearly distinguished from  $\Omega_{\text{GW}} \sim f^3$  already with present datasets. Our analysis applies to any GW source that is active before QCD confinement (i.e.  $T \gtrsim \text{GeV}$ , see also App. C), and provides a much-needed signature to help determining whether the detected SGWB is of cosmological or astrophysical origin. If the SMBHBs model (or a different CGW signal) is preferred, then our work should prove useful in the future to disentangle additional contributions from cosmological sources (see e.g. [89, 90] for a recent discussion).

We have shown that, despite the CMB bound on  $\Delta N_{\text{eff}}$  [85], a CT spectrum can explain the PTA signal. We quantitatively assessed it to be strongly favored over the commonly employed  $f^3$  approximation in the IPTA-DR2 dataset, while we have used the latest posteriors reported by NG15 and EPTA-DR2 [2, 4] to argue that a CT is likely also significantly preferred over the  $\alpha = -\frac{2}{3}$  power law in these new datasets.

The detection of such a signal would have dramatic implications for particle physics, most likely pointing to the breaking of a (global or gauge) symmetry in a dark sector (DS), for instance via a PT (or causing the annihilation of domain walls for discrete symmetries) at temperatures  $T \gtrsim \text{GeV}$ . Some macroscopic properties of the corresponding sub-Hubble GW source can be estimated rather model-independently (see also App. C). Its contribution to the total energy density at the temperature  $T_{\star}$  corresponding to the peak frequency  $f_{\star}$ , denoted by  $\alpha_{\star} \equiv [\rho_{\text{DS}}/(3H^2 M_p^2)]_{T=T_{\star}}$ , sets the peak

amplitude of the signal as (see e.g. [55])

$$\Omega_{\text{CGW}}(f_\star)h^2 \simeq 10^{-8} \epsilon_\star \left( \frac{74}{g_\star(T_\star)} \right)^{1/3} \left( \frac{\alpha_\star/(1+\alpha_\star)}{0.14} \right)^2, \quad (8)$$

where  $\epsilon_\star \lesssim 1$  encodes model-dependent suppressions due to the sub-Hubble size of the source and its possibly subluminal velocity, among other effects. Notice that we have normalized  $g_\star(T_\star)$  to its value at  $T_\star \simeq 1$  GeV. For simple power-law signals below the peak frequency  $f_\star$ , combining with Eq. (5) one has

$$\alpha_\star \simeq 0.35 \epsilon_\star^{-\frac{1}{2}} \left( \frac{g_\star(T_\star)}{74} \right)^{\frac{1}{6}} \left( \frac{A_{\text{CGW}}}{10^{-14}} \right) \left( \frac{f_\star}{f_{\text{yr}}} \right)^{n_T/2}, \quad (9)$$

for  $\alpha_\star \ll 1$ . As above, this estimate can also be used as a lower bound on  $\alpha_\star$  for CT signals, by replacing  $f_\star \rightarrow f_{\text{CT}}, A_{\text{CGW}} \rightarrow A_{\text{CT}}$ . The posteriors ( $2\sigma$ ) in Fig. 3 then imply the lower bound  $\alpha_\star \gtrsim (0.1 - 0.4)\epsilon_\star^{-1/2}$ , for  $15 \text{ nHz} \lesssim f_{\text{CT}} \lesssim f_{\text{yr}}$ . The required fraction is even larger for larger  $f_{\text{CT}}$ . This may be problematic for sources with  $\epsilon_\star \ll 1$ , as the DS would then dominate over the SM background ( $\alpha_\star \simeq 1$ ), and thus suggests that the source should be relativistic and Hubble-sized. We discuss further the scenario of a PT and its challenges in App. C (see [23] for the case of domain walls, and [25, 91] for previous discussions on PTs and NANOGrav).

Regardless, such a large abundance is currently (at  $2\sigma$ ) constrained by CMB observations, if it remains in dark ultrarelativistic species, since it contributes (see e.g. [23])

$$\Delta N_{\text{eff}}^{\text{DS}} \simeq 0.28 \left( \frac{74}{g_\star(T_\star)} \right)^{1/3} \left( \frac{\alpha_\star}{0.1} \right). \quad (10)$$

This conclusion is slightly alleviated for non-CT CGW signals, since one has a  $2\sigma$  lower bound  $\log_{10} A_{\text{CGW}} \gtrsim -14.6$  from NG15, see Fig. 3, to explain the current excess, thus requiring  $\alpha_\star \gtrsim 0.07\epsilon_\star^{-1/2}$ . Current and upcoming CMB and LSS surveys [86–88, 92] will be able to more decisively confirm or exclude the DS origin by probing down to  $\alpha_\star \gtrsim 0.03$  at  $2\sigma$ .

Such constraints are avoided if the dark sector rapidly transfers its energy density to the SM bath or if the source is part of the SM (if e.g. QCD confinement proceeds via a first order PT in the early Universe, although this scenario requires additional ingredients, see e.g. [93]). Interestingly, the required couplings between the SM and the dark sector may be additionally probed at colliders, laboratory experiments and astrophysical environments.

Finally, in our work we have conservatively employed the SM prediction for the EoS of the Universe. We

notice that the measurement of the CT at PTAs offers a probe of the whole cosmological expansion history up to  $T_{\text{QCD}}$ , as encapsulated by Eq. (4). Modifications to the CT could occur in BSM scenarios where  $w(T)$ ,  $g_\star(T)$  or  $f_{\text{FS}}$  are varied, or if the Universe undergoes a phase of matter domination below the QCD crossover (we present a search for this scenario in App. D). Additionally, PTAs also provide the opportunity to test the EoS of hot QCD matter in the early Universe (see e.g. [93, 94]), in the presence of a CT signal.

Overall, a near-future detection of a SGWB at PTAs could disclose a unique window around the epoch of the QCD crossover. As highlighted in this paper, this coincidence of scales provides a robust feature to assist in the discrimination between the astrophysical and cosmological origin of the SGWB.

## Acknowledgments

We thank Peter Graham, Antonio Junior Iovino, Ville Vaskonen and Hardi Veermäe for discussions, Zoltan Haiman for useful correspondence, and Valerie Domcke, Anson Hook and Gustavo Marques-Tavares for comments on the draft. We acknowledge use of the publicly available codes `enterprise` [95], `enterprise_extensions` [96] and `PTMCMC` [97] as well as of the free spectrum chains publicly provided by the `IPTA-DR2` collaboration. G.F. acknowledges financial support provided under the European Union’s H2020 ERC, Starting Grant agreement no. DarkGRA–757480 and under the MIUR PRIN programme, and support from the Amaldi Research Center funded by the MIUR program “Dipartimento di Eccellenza” (CUP: B81I18001170001). This work was supported by the EU Horizon 2020 Research and Innovation Programme under the Marie Skłodowska-Curie Grant Agreement No. 101007855 and additional financial support provided by “Progetti per Avvio alla Ricerca - Tipo 2”, protocol number AR2221816C515921. D.R. is supported in part by NSF Grant PHY-2014215, DOE HEP QuantISED award #100495, and the Gordon and Betty Moore Foundation Grant GBMF7946. The work of F.R. is partly supported by the grant RYC2021-031105-I from the Ministerio de Ciencia e Innovación (Spain). F.R. thanks the Galileo Galilei Institute in Florence and the organizers of the New Physics@Korea Institute for kind hospitality during the completion of this work.

- 
- [1] G. Agazie *et al.* (NANOGrav), (2023), [arXiv:2306.16217 \[astro-ph.HE\]](https://arxiv.org/abs/2306.16217).  
 [2] G. Agazie *et al.* (NANOGrav), (2023),

- [arXiv:2306.16213 \[astro-ph.HE\]](https://arxiv.org/abs/2306.16213).  
 [3] J. Antoniadis *et al.* (EPTA), (2023), [arXiv:2306.16224 \[astro-ph.HE\]](https://arxiv.org/abs/2306.16224).

- [4] J. Antoniadis *et al.* (EPTA), (2023), arXiv:2306.16214 [astro-ph.HE].
- [5] A. Zic *et al.* (PPTA), (2023), arXiv:2306.16230 [astro-ph.HE].
- [6] D. Reardon *et al.* (PPTA), (2023), arXiv:2306.16215 [astro-ph.HE].
- [7] H. Xu *et al.* (CPTA), (2023), arXiv:2306.16216 [astro-ph.HE].
- [8] Z. Arzoumanian *et al.* (NANOGrav), *Astrophys. J. Lett.* **905**, L34 (2020), arXiv:2009.04496 [astro-ph.HE].
- [9] B. Goncharov *et al.*, *Astrophys. J. Lett.* **917**, L19 (2021), arXiv:2107.12112 [astro-ph.HE].
- [10] S. Chen *et al.*, *Mon. Not. Roy. Astron. Soc.* **508**, 4970 (2021), arXiv:2110.13184 [astro-ph.HE].
- [11] J. Antoniadis *et al.*, *Mon. Not. Roy. Astron. Soc.* **510**, 10.1093/mnras/stab3418 (2022), arXiv:2201.03980 [astro-ph.HE].
- [12] S. Burke-Spolaor *et al.*, *Astron. Astrophys. Rev.* **27**, 5 (2019), arXiv:1811.08826 [astro-ph.HE].
- [13] N. S. Pol *et al.* (NANOGrav), *Astrophys. J. Lett.* **911**, L34 (2021), arXiv:2010.11950 [astro-ph.HE].
- [14] G. Agazie *et al.* (NANOGrav), (2023), arXiv:2306.16220 [astro-ph.HE].
- [15] J. Antoniadis *et al.* (EPTA), (2023), arXiv:2306.16227 [astro-ph.HE].
- [16] H. Middleton, A. Sesana, S. Chen, A. Vecchio, W. Del Pozzo, and P. A. Rosado, *Mon. Not. Roy. Astron. Soc.* **502**, L99 (2021), arXiv:2011.01246 [astro-ph.HE].
- [17] E. Witten, *Phys. Rev. D* **30**, 272 (1984).
- [18] A. Vilenkin, *Phys. Rev. D* **23**, 852 (1981).
- [19] S. Matarrese, S. Mollerach, and M. Bruni, *Phys. Rev. D* **58**, 043504 (1998), arXiv:astro-ph/9707278.
- [20] L. Bian, R.-G. Cai, J. Liu, X.-Y. Yang, and R. Zhou, *Phys. Rev. D* **103**, L081301 (2021), arXiv:2009.13893 [astro-ph.CO].
- [21] Z. Arzoumanian *et al.* (NANOGrav), *Phys. Rev. Lett.* **127**, 251302 (2021), arXiv:2104.13930 [astro-ph.CO].
- [22] X. Xue *et al.*, *Phys. Rev. Lett.* **127**, 251303 (2021), arXiv:2110.03096 [astro-ph.CO].
- [23] R. Z. Ferreira, A. Notari, O. Pujolas, and F. Rompineve, *JCAP* **02**, 001, arXiv:2204.04228 [astro-ph.CO].
- [24] V. Dandoy, V. Domcke, and F. Rompineve, (2023), arXiv:2302.07901 [astro-ph.CO].
- [25] T. Bringmann, P. F. Depta, T. Konstandin, K. Schmidt-Hoberg, and C. Tassilo, (2023), arXiv:2306.09411 [astro-ph.CO].
- [26] A. Afzal *et al.* (NANOGrav), (2023), arXiv:2306.16219 [astro-ph.HE].
- [27] Y. Nakai, M. Suzuki, F. Takahashi, and M. Yamada, *Phys. Lett. B* **816**, 136238 (2021), arXiv:2009.09754 [astro-ph.CO].
- [28] V. Vaskonen and H. Veermäe, *Phys. Rev. Lett.* **126**, 051303 (2021), arXiv:2009.07832 [astro-ph.CO].
- [29] V. De Luca, G. Franciolini, and A. Riotto, *Phys. Rev. Lett.* **126**, 041303 (2021), arXiv:2009.08268 [astro-ph.CO].
- [30] A. Neronov, A. Roper Pol, C. Caprini, and D. Semikoz, *Phys. Rev. D* **103**, 041302 (2021), arXiv:2009.14174 [astro-ph.CO].
- [31] A. Roper Pol, C. Caprini, A. Neronov, and D. Semikoz, *Phys. Rev. D* **105**, 123502 (2022), arXiv:2201.05630 [astro-ph.CO].
- [32] J. Ellis and M. Lewicki, *Phys. Rev. Lett.* **126**, 041304 (2021), arXiv:2009.06555 [astro-ph.CO].
- [33] S. Blasi, V. Brdar, and K. Schmitz, *Phys. Rev. Lett.* **126**, 041305 (2021), arXiv:2009.06607 [astro-ph.CO].
- [34] S. Vagnozzi, *Mon. Not. Roy. Astron. Soc.* **502**, L11 (2021), arXiv:2009.13432 [astro-ph.CO].
- [35] J. J. Blanco-Pillado, K. D. Olum, and J. M. Wachter, *Phys. Rev. D* **103**, 103512 (2021), arXiv:2102.08194 [astro-ph.CO].
- [36] Y. Aoki, G. Endrodi, Z. Fodor, S. D. Katz, and K. K. Szabo, *Nature* **443**, 675 (2006), arXiv:hep-lat/0611014.
- [37] S. Borsanyi *et al.*, *Nature* **539**, 69 (2016), arXiv:1606.07494 [hep-lat].
- [38] Y. Watanabe and E. Komatsu, *Phys. Rev. D* **73**, 123515 (2006), arXiv:astro-ph/0604176.
- [39] S. Schettler, T. Boeckel, and J. Schaffner-Bielich, *Phys. Rev. D* **83**, 064030 (2011), arXiv:1010.4857 [astro-ph.CO].
- [40] A. Hook, G. Marques-Tavares, and D. Racco, *JHEP* **02**, 117, arXiv:2010.03568 [hep-ph].
- [41] D. Brzeminski, A. Hook, and G. Marques-Tavares, *JHEP* **11**, 061, arXiv:2203.13842 [hep-ph].
- [42] M. Loverde and Z. J. Weiner, *JCAP* **02**, 064, arXiv:2208.11714 [astro-ph.CO].
- [43] B. B. P. Perera *et al.*, *Mon. Not. Roy. Astron. Soc.* **490**, 4666 (2019), arXiv:1909.04534 [astro-ph.HE].
- [44] N. Seto and J. Yokoyama, *J. Phys. Soc. Jap.* **72**, 3082 (2003), arXiv:gr-qc/0305096.
- [45] S. Weinberg, *Phys. Rev. D* **69**, 023503 (2004), arXiv:astro-ph/0306304.
- [46] L. A. Boyle and P. J. Steinhardt, *Phys. Rev. D* **77**, 063504 (2008), arXiv:astro-ph/0512014.
- [47] L. A. Boyle and A. Buonanno, *Phys. Rev. D* **78**, 043531 (2008), arXiv:0708.2279 [astro-ph].
- [48] R. Jinno, T. Moroi, and K. Nakayama, *Phys. Rev. D* **86**, 123502 (2012), arXiv:1208.0184 [astro-ph.CO].
- [49] C. Caprini *et al.*, *JCAP* **04**, 001, arXiv:1512.06239 [astro-ph.CO].
- [50] G. Barenboim and W.-I. Park, *Phys. Lett. B* **759**, 430 (2016), arXiv:1605.03781 [astro-ph.CO].
- [51] M. Geller, A. Hook, R. Sundrum, and Y. Tsai, *Phys. Rev. Lett.* **121**, 201303 (2018), arXiv:1803.10780 [hep-ph].
- [52] K. Saikawa and S. Shirai, *JCAP* **1805**, 035, arXiv:1803.01038 [hep-ph].
- [53] Y. Cui, M. Lewicki, D. E. Morrissey, and J. D. Wells, *JHEP* **01**, 081, arXiv:1808.08968 [hep-ph].
- [54] R. R. Caldwell, T. L. Smith, and D. G. E. Walker, *Phys. Rev. D* **100**, 043513 (2019), arXiv:1812.07577 [astro-ph.CO].
- [55] C. Caprini and D. G. Figueroa, *Class. Quant. Grav.* **35**, 163001 (2018), arXiv:1801.04268 [astro-ph.CO].
- [56] R.-G. Cai, S. Pi, and M. Sasaki, *Phys. Rev. D* **102**, 083528 (2020), arXiv:1909.13728 [astro-ph.CO].
- [57] F. D’Eramo and K. Schmitz, *Phys. Rev. Research* , 013010 (2019), arXiv:1904.07870 [hep-ph].
- [58] N. Bernal and F. Hajkarim, *Phys. Rev. D* **100**, 063502 (2019), arXiv:1905.10410 [astro-ph.CO].
- [59] D. G. Figueroa and E. H. Tanin, *JCAP* **1908**, 011, arXiv:1905.11960 [astro-ph.CO].
- [60] P. Auclair *et al.*, *JCAP* **04**, 034, arXiv:1909.00819 [astro-ph.CO].
- [61] C.-F. Chang and Y. Cui, *Phys. Dark Univ.* **29**, 100604 (2020), arXiv:1910.04781 [hep-ph].
- [62] F. Hajkarim and J. Schaffner-Bielich, *Phys. Rev. D* **101**,

- 043522 (2020), arXiv:1910.12357 [hep-ph].
- [63] C. Caprini *et al.*, *JCAP* **03**, 024, arXiv:1910.13125 [astro-ph.CO].
- [64] Y. Gouttenoire, G. Servant, and P. Simakachorn, *JCAP* **07**, 032, arXiv:1912.02569 [hep-ph].
- [65] Y. Gouttenoire, G. Servant, and P. Simakachorn, *JCAP* **07**, 016, arXiv:1912.03245 [hep-ph].
- [66] G. Domènech, *Int. J. Mod. Phys. D* **29**, 2050028 (2020), arXiv:1912.05583 [gr-qc].
- [67] H.-K. Guo, K. Sinha, D. Vagie, and G. White, *JCAP* **01**, 001, arXiv:2007.08537 [hep-ph].
- [68] J. Ellis, M. Lewicki, and V. Vaskonen, *JCAP* **11**, 020, arXiv:2007.15586 [astro-ph.CO].
- [69] S. Blasi, V. Brdar, and K. Schmitz, *Phys. Rev. Res.* **2**, 043321 (2020), arXiv:2004.02889 [hep-ph].
- [70] G. Domènech, S. Pi, and M. Sasaki, *JCAP* **08**, 017, arXiv:2005.12314 [gr-qc].
- [71] R. Allahverdi *et al.*, *The Open Journal of Astrophysics* **4**, 1 (2021), arXiv:2006.16182 [astro-ph.CO].
- [72] J. Berger, A. Bhoonah, and B. Padhi, (2023), arXiv:2306.07283 [hep-ph].
- [73] M. B. Hindmarsh, M. Lüben, J. Lumma, and M. Pauly, *SciPost Phys. Lect. Notes* **24**, 1 (2021), arXiv:2008.09136 [astro-ph.CO].
- [74] P. Athron, C. Balázs, A. Fowlie, L. Morris, and L. Wu, (2023), arXiv:2305.02357 [hep-ph].
- [75] R. w. Hellings and G. s. Downs, *Astrophys. J. Lett.* **265**, L39 (1983).
- [76] Z. Haiman, Z. Haiman, B. Kocsis, B. Kocsis, K. Menou, and K. Menou, *Astrophys. J.* **700**, 1952 (2009), [Erratum: *Astrophys. J.* 937, 129 (2022)], arXiv:0904.1383 [astro-ph.CO].
- [77] B. Kocsis and A. Sesana, *Mon. Not. Roy. Astron. Soc.* **411**, 1467 (2011), arXiv:1002.0584 [astro-ph.CO].
- [78] Z. Pan, Z. Lyu, and H. Yang, *Phys. Rev. D* **104**, 063007 (2021), arXiv:2104.01208 [astro-ph.HE].
- [79] J. Ellis, M. Fairbairn, G. Hütsi, M. Raidal, J. Urrutia, V. Vaskonen, and H. Veermäe, (2023), arXiv:2301.13854 [astro-ph.CO].
- [80] M. M. Kozhikkal, S. Chen, G. Theureau, M. Habouzit, and A. Sesana, (2023), arXiv:2305.18293 [astro-ph.CO].
- [81] E. S. Phinney, (2001), arXiv:astro-ph/0108028.
- [82] N. Aghanim *et al.* (Planck), *Astron. Astrophys.* **641**, A6 (2020), [Erratum: *Astron. Astrophys.* 652, C4 (2021)], arXiv:1807.06209 [astro-ph.CO].
- [83] D. Cutting, E. G. Escartin, M. Hindmarsh, and D. J. Weir, *Phys. Rev. D* **103**, 023531 (2021), arXiv:2005.13537 [astro-ph.CO].
- [84] R. Jinno, T. Konstandin, and H. Rubira, *JCAP* **04**, 014, arXiv:2010.00971 [astro-ph.CO].
- [85] C. J. Moore and A. Vecchio, *Nature Astron.* **5**, 1268 (2021), arXiv:2104.15130 [astro-ph.CO].
- [86] A. Aghamousa *et al.* (DESI), (2016), arXiv:1611.00036 [astro-ph.IM].
- [87] L. Amendola *et al.*, *Living Rev. Rel.* **21**, 2 (2018), arXiv:1606.00180 [astro-ph.CO].
- [88] K. Abazajian *et al.* (CMB-S4), (2022), arXiv:2203.08024 [astro-ph.CO].
- [89] A. R. Kaiser, N. S. Pol, M. A. McLaughlin, S. Chen, J. S. Hazboun, L. Z. Kelley, J. Simon, S. R. Taylor, S. J. Vigeland, and C. A. Witt, *Astrophys. J.* **938**, 115 (2022), arXiv:2208.02307 [astro-ph.CO].
- [90] G. Sato-Polito and M. Kamionkowski, (2023), arXiv:2305.05690 [astro-ph.CO].
- [91] Y. Bai and M. Korwar, *Phys. Rev. D* **105**, 095015 (2022), arXiv:2109.14765 [hep-ph].
- [92] P. Ade *et al.* (Simons Observatory), *JCAP* **02**, 056, arXiv:1808.07445 [astro-ph.CO].
- [93] D. Bödeker, F. Kühnel, I. M. Oldengott, and D. J. Schwarz, *Phys. Rev. D* **103**, 063506 (2021), arXiv:2011.07283 [astro-ph.CO].
- [94] P. Achenbach *et al.*, (2023), arXiv:2303.02579 [hep-ph].
- [95] J. A. Ellis, M. Vallisneri, S. R. Taylor, and P. T. Baker, *Enterprise: Enhanced numerical toolbox enabling a robust pulsar inference suite*, Zenodo (2020).
- [96] S. R. Taylor, P. T. Baker, J. S. Hazboun, J. Simon, and S. J. Vigeland, *enterprise\_extensions* (2021), v2.3.3.
- [97] J. Ellis and R. van Haasteren, *jellis18/ptmcmcsampler: Official release* (2017).
- [98] C. Patrignani *et al.* (Particle Data Group), *Chin. Phys. C* **40**, 100001 (2016).
- [99] E. W. Kolb and M. S. Turner, *The Early Universe*, Vol. 69 (1990).
- [100] S. Borsányi, Z. Fodor, J. N. Guenther, R. Kara, S. D. Katz, P. Parotto, A. Pásztor, C. Ratti, and K. K. Szabó, *Phys. Rev. Lett.* **126**, 232001 (2021), arXiv:2102.06660 [hep-lat].
- [101] D. E. Kaplan, M. A. Luty, and K. M. Zurek, *Phys. Rev. D* **79**, 115016 (2009), arXiv:0901.4117 [hep-ph].
- [102] R. Foot and R. R. Volkas, *Phys. Rev. D* **68**, 021304 (2003), arXiv:hep-ph/0304261.
- [103] R. Foot and R. R. Volkas, *Phys. Rev. D* **69**, 123510 (2004), arXiv:hep-ph/0402267.
- [104] S. J. Lonsdale and R. R. Volkas, *Phys. Rev. D* **90**, 083501 (2014), [Erratum: *Phys. Rev. D* 91, 129906 (2015)], arXiv:1407.4192 [hep-ph].
- [105] S. J. Lonsdale, *Phys. Rev. D* **91**, 125019 (2015), arXiv:1412.1894 [hep-ph].
- [106] S. J. Lonsdale and R. R. Volkas, *Phys. Rev. D* **97**, 103510 (2018), arXiv:1801.05561 [hep-ph].
- [107] C. Murgui and K. M. Zurek, *Phys. Rev. D* **105**, 095002 (2022), arXiv:2112.08374 [hep-ph].
- [108] P. Baratella, A. Pomarol, and F. Rompineve, *JHEP* **03**, 100, arXiv:1812.06996 [hep-ph].
- [109] W. DeRocco, P. W. Graham, D. Kasen, G. Marques-Tavares, and S. Rajendran, *Phys. Rev. D* **100**, 075018 (2019), arXiv:1905.09284 [hep-ph].
- [110] V. Acquaviva, N. Bartolo, S. Matarrese, and A. Riotto, *Nucl. Phys. B* **667**, 119 (2003), arXiv:astro-ph/0209156.
- [111] S. Mollerach, D. Harari, and S. Matarrese, *Phys. Rev. D* **69**, 063002 (2004), arXiv:astro-ph/0310711.
- [112] D. Baumann, P. J. Steinhardt, K. Takahashi, and K. Ichiki, *Phys. Rev. D* **76**, 084019 (2007), arXiv:hep-th/0703290 [hep-th].
- [113] J. R. Espinosa, D. Racco, and A. Riotto, *JCAP* **1809** (09), 012, arXiv:1804.07732 [hep-ph].
- [114] K. Kohri and T. Terada, *Phys. Rev. D* **97**, 123532 (2018), arXiv:1804.08577 [gr-qc].
- [115] R. Saito and J. Yokoyama, *Phys. Rev. Lett.* **102**, 161101 (2009), [Erratum: *Phys. Rev. Lett.* 107, 069901 (2011)], arXiv:0812.4339 [astro-ph].
- [116] K. Kohri and T. Terada, *Phys. Lett. B* **813**, 136040 (2021), arXiv:2009.11853 [astro-ph.CO].
- [117] S. Sugiyama, V. Takhistov, E. Vitagliano, A. Kusenko, M. Sasaki, and M. Takada, *Phys. Lett. B* **814**, 136097 (2021), arXiv:2010.02189 [astro-ph.CO].
- [118] G. Domènech and S. Pi, *Sci. China Phys. Mech. Astron.* **65**, 230411 (2022), arXiv:2010.03976 [astro-ph.CO].

- [119] K. Inomata, M. Kawasaki, K. Mukaida, and T. T. Yanagida, *Phys. Rev. Lett.* **126**, 131301 (2021), [arXiv:2011.01270 \[astro-ph.CO\]](#).
- [120] G. Franciolini and A. Urbano, *Phys. Rev. D* **106**, 123519 (2022), [arXiv:2207.10056 \[astro-ph.CO\]](#).
- [121] G. Franciolini, I. Musco, P. Pani, and A. Urbano, *Phys. Rev. D* **106**, 123526 (2022), [arXiv:2209.05959 \[astro-ph.CO\]](#).
- [122] G. Ferrante, G. Franciolini, A. Iovino, Junior., and A. Urbano [10.1088/1475-7516/2023/06/057](#) (2023), [arXiv:2305.13382 \[astro-ph.CO\]](#).
- [123] M. Sasaki, T. Suyama, T. Tanaka, and S. Yokoyama, *Class. Quant. Grav.* **35**, 063001 (2018), [arXiv:1801.05235 \[astro-ph.CO\]](#).
- [124] B. Carr, K. Kohri, Y. Sendouda, and J. Yokoyama, *Rept. Prog. Phys.* **84**, 116902 (2021), [arXiv:2002.12778 \[astro-ph.CO\]](#).
- [125] G. Franciolini, A. J. Iovino, V. Vaskonen, and H. Veermäe, in preparation.
- [126] K. T. Abe, Y. Tada, and I. Ueda, *JCAP* **06**, 048, [arXiv:2010.06193 \[astro-ph.CO\]](#).
- [127] M. Gorghetto, E. Hardy, and H. Nicolaescu, *JCAP* **06**, 034, [arXiv:2101.11007 \[hep-ph\]](#).
- [128] R. Jinno and M. Takimoto, *Phys. Rev. D* **95**, 024009 (2017), [arXiv:1605.01403 \[astro-ph.CO\]](#).
- [129] M. Hindmarsh, S. J. Huber, K. Rummukainen, and D. J. Weir, *Phys. Rev. D* **96**, 103520 (2017), [Erratum: *Phys.Rev.D* 101, 089902 (2020)], [arXiv:1704.05871 \[astro-ph.CO\]](#).
- [130] A. Lewis, (2019), [arXiv:1910.13970 \[astro-ph.IM\]](#).

### A. Relation between frequency today and temperature at horizon crossing

We derive here the present frequencies corresponding to modes crossing the horizon at a given time, in order to clarify a potential confusion with the typical peak frequency of primordial SGWBs and to highlight the coincidence of frequencies probed by PTAs and modes corresponding to the QCD crossover.

The frequency (redshifted to its present day value) of modes crossing the horizon at a given epoch can be simply derived as follows. We impose that, at the temperature of horizon crossing one has  $k = aH$ ,

$$f(T) \equiv \frac{k}{2\pi a_0} = \frac{a(T)}{a_0} \frac{H(T)}{2\pi}. \quad (\text{A1})$$

Using the conservation of entropy  $g_{*,s}(T)T^3 a^3(T) = \text{constant}$ , the ratio of scale factors between GW production at a temperature  $T$ , and the present time at  $T_0$ , is

$$\begin{aligned} \frac{a(T)}{a_0} &= \left( \frac{g_{*,s}(T_0)}{g_{*,s}(T)} \right)^{1/3} \left( \frac{T_0}{T} \right) \simeq \\ &\simeq 8.0 \times 10^{-14} \left( \frac{g_{*,s}(T)}{100} \right)^{-1/3} \left( \frac{T}{\text{GeV}} \right)^{-1}, \end{aligned} \quad (\text{A2})$$

where we have used  $T_0 \simeq 2.4 \times 10^{-13}$  GeV for the photon temperature today [98] and  $g_{*,s}(T_0) \simeq 3.91$

for the Standard Model degrees of freedom with three light neutrino species [99]. Additionally, employing the Friedmann equation  $H^2 = \rho/(3M_p^2)$ , where  $M_p \equiv \sqrt{8\pi G_N} \simeq 2.4 \cdot 10^{18}$  GeV is the reduced Planck mass, the energy density in a radiation dominated era  $\rho = (\pi^2/30)g_*(T)T^4$  and  $g_{*,s}(T) \simeq g_*(T)$ , one obtains Eq. (4).

If one considers the emission of GWs from a cosmological phase transition (or from e.g. domain wall annihilation), the characteristic frequency  $f_*$  of the SGWB, i.e. the frequency at which one expects the SGWB to peak, is located around the inverse typical time or length scale of the system, which is the inverse of the duration of the PT or of the bubble size, depending on the details of the source. Following Ref. [55], we set  $k_*/a_* \simeq 2\pi\beta$ , where  $\beta$  is the inverse of the nucleation timescale. Therefore, one obtains the characteristic frequency today as

$$f_{*,0} \simeq 24 \text{ nHz} \cdot \left( \frac{\beta}{H_*} \right) \left( \frac{g_*(T_*)}{100} \right)^{1/6} \left( \frac{T_*}{150 \text{ MeV}} \right). \quad (\text{A3})$$

Notice that this frequency is larger by a factor of  $2\pi$  than the frequency in Eq. (4) corresponding to horizon crossing at a given  $T$ , because they refer to two different physical quantities. Eq. (A3) gives the typical peak  $f_*$  of the SGWB and identifies the wavenumber  $k = 2\pi/\lambda = 2\pi f$  associated to the excitation of a GW over a period  $f^{-1} \simeq \beta^{-1}$ , whereas Eq. (4) determines the wavenumber  $k = a(T)H(T)$  crossing the Hubble radius at a given time, and allows to fix the boundary  $f_{\text{CT}}$  of the CT.

### B. Tabulated causality tail

This Appendix provides more details about the CT that we compute and use for our analysis. For completeness, we provide a summary of the dynamics for low frequency GW modes excited by a local, causality-limited source in the early Universe (see [40] for details). The equations of motion in conformal time  $\tau$  for a GW mode  $h_k(\tau)$  sourced by sector with energy density  $\rho_s$  and dimensionless anisotropic stress  $\Pi$  read (we understand the space-time tensor indices and the polarisation  $(+, \times)$  indices for both the GW and source)

$$h_k'' + 2\mathcal{H} h_k' + \frac{k^2}{a^2} h_k = a^2 \frac{4\rho_s}{3M_p^2} \Pi(\tau, k) \equiv J(\tau, k), \quad (\text{B1})$$

where  $\mathcal{H} = a'/a$  is the conformal Hubble time and  $'$  denotes conformal time derivatives. At small  $k$ , the source takes a simple and universal form when it lasts for a finite amount of time (up to a time  $\tau_*$ ) and has a finite correlation length ( $\lesssim 2\pi/k_*$ , where  $k_* \equiv \mathcal{H}(\tau_*)$  is the mode crossing the Hubble radius at  $\tau_*$ ). This corresponds to GW periods longer than the duration of the source, so that the time dependence of the source is basically a Dirac delta function, and to wavenumbers where the power spectrum of the source is independent

of  $k$  (and is given by white noise, meaning that sources in different Hubble patches are uncorrelated). Therefore, in this limit  $J(\tau, k) \rightarrow J_\star \delta(\tau - \tau_\star)$ , so that an initially vanishing GW mode gets a velocity  $h'_k = J_\star$  shortly after  $\tau_\star$ , and thereafter evolves according to

$$h''_k(\tau) + 2\mathcal{H}(\tau)h'_k(\tau) + \frac{k^2}{a^2(\tau)}h_k(\tau) = 0, \quad (\text{B2})$$

$$h_k(\tau_\star) = 0, \quad h'_k(\tau_\star) = J_\star.$$

We solve Eq. (B2) for a wide range of momenta  $k < k_\star$  by accounting for the expansion history of  $\Lambda$ CDM with the SM content around the QCD crossover. We notice that a positive detection of these features on the CT allows to confirm that the cosmological expansion history up to  $T \sim T_{\text{QCD}}$  has followed the predictions of  $\Lambda$ CDM, and possible deviations would hint at a different evolution of the scale factor. We can then compute the GW power spectrum  $P_h \sim \langle (a(\tau)h_k(\tau))^2 \rangle$  after horizon crossing, and  $\Omega_{\text{CT}} \propto f^5 P_h(f)$  [40].

To include the effect of free-streaming (high-frequency) GWs on the CT, one starts with the modification on  $\Omega_{\text{GW}}h^2 = S_1(f)f^{16f_{\text{FS}}/5}$ . Here  $S_1$  is a function that describes the CT for  $f_{\text{FS}} = 0$ . Then we transform to the characteristic strain  $h_c(f)$ , as follows

$$h_c(f) = 1.26 \cdot 10^{-9} \left( \frac{\text{nHz}}{f} \right) \sqrt{\Omega_{\text{GW}}h^2}, \quad (\text{B3})$$

which can then be rewritten as

$$h_c(f) = A_{\text{CT}} \frac{\mathcal{S}(f)}{\mathcal{S}(f_{\text{CT}})} \left( \frac{f_{\text{CT}}}{f} \right)^{-\frac{8}{5}f_{\text{FS}}}, \quad (\text{B4})$$

where  $\mathcal{S}$  is the function tabulated in Tab. II. When  $f_{\text{CT}} = f_{\text{YR}}$ , then  $A_{\text{CT}}$  is the amplitude of the signal at  $f = \text{yR}^{-1}$ , as in our paper, whereas generally it is just the amplitude at  $f_{\text{CT}}$ . With this notation, the  $\Delta N_{\text{eff}}$  constraint on  $\Omega_{\text{GW}}h^2$  at  $f_{\text{CT}}$  reads

$$\Omega_{\text{GW}}(f_{\text{CT}})h^2 \simeq 1.6 \cdot 10^{-6} \left( \frac{\Delta N_{\text{eff}}^{\text{CGW}}}{0.28} \right), \quad (\text{B5})$$

which implies

$$A_{\text{CT}} = 5 \cdot 10^{-14} \left( \frac{f_{\text{YR}}}{f_{\text{CT}}} \right) \sqrt{\frac{\Delta N_{\text{eff}}}{0.28}}. \quad (\text{B6})$$

Now let us relate  $f_{\text{FS}}$  to  $A_{\text{CT}}$ . The definition of  $\Delta N_{\text{eff}}$  is

$$\Delta N_{\text{eff}} = \frac{\rho_{\text{GW}}}{\rho_{\nu,1}} \Big|_{\text{CMB}}, \quad (\text{B7})$$

where  $\rho_{\nu,1}$  is the energy density in one neutrino species. At CMB, this is related to the total energy density in radiation by

$$\rho_{\nu,1} = \rho_{\text{rad}} \left( \frac{T_\nu}{T_{\text{rad}}} \right)^4 \left( \frac{g_\nu}{g_{\text{rad}}} \right) = \rho_{\text{rad}} \left( \frac{4}{11} \right)^{4/3} \frac{2 \cdot \frac{7}{8}}{g_{\star, \text{CMB}}}. \quad (\text{B8})$$

$f$ [nHz]	$\mathcal{S}(f)$ (Eq. 6)	$\Omega_{\text{CT}}(f)$ (arb. units)
1.00	0.300	0.0000897
1.22	0.325	0.000157
1.49	0.353	0.000276
1.82	0.382	0.000482
2.23	0.413	0.000841
2.72	0.444	0.00145
3.32	0.470	0.00243
4.06	0.491	0.00397
4.96	0.512	0.00642
6.06	0.530	0.0103
7.41	0.559	0.0171
9.05	0.600	0.0293
11.1	0.646	0.0508
13.5	0.700	0.089
16.5	0.760	0.156
20.2	0.825	0.276
24.6	0.898	0.486
30.1	0.978	0.861
36.7	1.07	1.53
44.9	1.17	2.73
54.8	1.28	4.89
67.	1.40	8.8
81.9	1.54	15.9
100	1.70	28.7

TABLE II. Tabulated values for the Causality Tail computed in this work, accounting for the effect of the SM QCD phase transition. The last column assume negligible  $f_{\text{FS}}$ .

Additionally,  $\rho_{\text{GW}}/\rho_{\text{rad}} \propto g_\star g_{\star, \text{s}}^{-4/3}$  from entropy conservation, therefore we have

$$\Delta N_{\text{eff}} = \left( \frac{11}{4} g_{\star, \text{s, CMB}} \right)^{\frac{4}{3}} \frac{g_\star(T_{\text{CT}})^{1/3}}{2 \cdot \frac{7}{8}} \cdot f_{\text{FS}} \simeq 13.7 g_\star^{-1/3} f_{\text{FS}}, \quad (\text{B9})$$

where  $f_{\text{FS}} = \rho_{\text{GW}}/\rho_{\text{rad}}$  and we assume that the background is always dominated by SM radiation between GW production and matter-radiation equality. Using the above relation between  $\Delta N_{\text{eff}}$  and  $\Omega_{\text{GW}}h^2$ , we then have

$$f_{\text{FS}} \simeq 0.086 \left( \frac{A_{\text{CT}}}{5 \cdot 10^{-14}} \right)^2 \left( \frac{g_\star(T_{\text{CT}})}{74} \right)^{1/3}, \quad (\text{B10})$$

where we have normalized  $g_\star$  to its value at temperatures corresponding to  $f_{\text{CT}} = f_{\text{YR}}$ . Plugging this into (B4), we obtain the GW-altered causality-tail characteristic strain as a function of two parameters:  $f_{\text{CT}}$  and  $A_{\text{CT}}$ . In our runs, we shall fix  $f_{\text{CT}}$  and we are thus left with only one free parameter.

Table II contains the tabulated result, parameterised through the function  $\mathcal{S}(f)$  defined in Eq. (6), which expresses the characteristic strain as a function of frequency in the PTA range. This function can be directly used as an input for Bayesian parameter estimation. We also include the tabulated curve for the corresponding  $\Omega_{\text{CT}}(f) \propto f^2 \mathcal{S}(f)^2$  shown in Fig. 1.

### C. Implications for Particle Physics

We collect here various important considerations from cosmology and particle physics related to our work, and in particular some consequences of the microscopical interpretation of the GW primordial signal. We focus especially on the SGWB generated by the prototypical example of a causality-limited signal, a first-order phase transition.

*a. Peak frequency for a causality-limited GW signal around the QCD phase transition.* In this work we are studying the impact of the QCD era<sup>2</sup> on modes that are excited by a local GW source when they are still outside the Hubble horizon, i.e.  $k_{\text{QCD}} \ll a(T_{\text{QCD}})H(T_{\text{QCD}})$ , where we denote by the subscript “QCD” quantities evaluated when the temperature of the universe was  $T = T_{\text{QCD}} \simeq 150$  MeV. The mode  $k_{\text{QCD}}$  corresponds to frequencies  $f_{\text{QCD}} \equiv k_{\text{QCD}}/(2\pi) \ll aH/(2\pi)$ . Therefore, for consistency, we have to require the emission of frequencies around  $f_{\text{QCD}} \approx 3$  nHz to take place when the corresponding modes were super-horizon, i.e. when the temperature of the universe was larger than  $T_{\text{QCD}}$ . Requiring  $f_{\text{QCD}}$  to be emitted at temperature larger than the QCD transition, forces the peak frequency to  $f_\star \gtrsim 24$  nHz  $(\beta/H_\star)$ , neglecting the small impact of the change of effective degrees of freedom. Hence, a detection of a CT signal at PTAs would necessarily imply  $T_\star \gtrsim 300$  MeV, or the peak of the signal would lie in the first PTA bins.

The possibility of a PT occurring in a DS not far from the SM QCD crossover might be motivated for example in proposals addressing the approximate coincidence of dark matter and baryonic energy density in the context of asymmetric dark matter [101–107].

*b. Constraints on the evolution of the dark sector responsible for the SGWB.* The GW signal investigated in our work is largely independent of the nature of the GW source, as long as the latter occurs on sub-horizon scales and is active only up to a definite epoch in the early Universe. While this is obviously a virtue, it also implies that the detection of a CT signal at PTAs would not be able to uniquely identify the microphysical mechanism which acts as a GW source. To this aim, complementary probes would then be essential.

Nonetheless, some general conclusions can be drawn from a detection of a CT, which apply to a broad class of sources. These necessarily involve physics beyond the SM, which can be organized in a non-specified dark sector (DS). Several scenarios of interest can then be described by using effective macroscopic parameters:

<sup>2</sup> The lattice results for  $g_{\star,s}(T)$  are obtained at vanishing baryon chemical potential, which corresponds to a vanishing baryon asymmetry at the QCD epoch,  $\eta_B \ll 1$ . Larger values are indeed expected to affect the EoS, see e.g. [100], therefore the CT. While still possible in principle, this scenario likely requires a late entropy injection that would also dilute any GW signal.

the temperature  $T_\star$  at which the GW source is active and the fraction of the (radiation) energy density that it comprises,  $\alpha_\star \equiv [\rho_{\text{DS}}/(3H^2 M_p^2)]_{T=T_\star}$ . The peak frequency of the GW signal at the time of emission is then determined by the inverse characteristic time scale of the source in units of the Hubble rate: this is given in Eq. (A3), where we can define in greater generality a dimensionless parameter  $\delta_\star \equiv f_\star/H_\star$  (that takes the specific form  $\beta/H_\star$  for PTs, while for domain walls in the scaling regime  $\delta_\star \simeq 1$ ). Typically, this time scale is smaller than or comparable to one Hubble time, thus  $\delta_\star \gtrsim 1$ . The peak amplitude of the signal today is then estimated as in (C1) (see e.g. [55]), which we report here for convenience

$$\Omega_{\text{CGW}}(f_{\star,0})h^2 \simeq 10^{-8} \epsilon_\star \left( \frac{74}{g_\star(T_\star)} \right)^{1/3} \left( \frac{\alpha_\star/(1+\alpha_\star)}{0.14} \right)^2, \quad (\text{C1})$$

where  $\epsilon_\star \lesssim 1$  generically scales as an inverse power of  $\delta_\star$  (depending on the microphysics of the source) and also account for additional signal-suppressing effects (such as subluminal velocities).

As mentioned in the main text, the required large fraction of energy density to fit the current excess cannot remain secluded from the SM bath below  $T_\star$  because of CMB and BBN constraints. This thus leaves only one possibility: the dark sector should deposit a significant amount of its energy density into the SM bath shortly after the emission of GWs.

This conclusion generically remains true when the source is a first order PT in a dark sector, even when the peak frequency lies among the first frequency bins of PTAs. Indeed, for PTs  $\delta_\star \simeq (\beta/H_\star) \geq 1$  is the rate of variation of the bubble nucleation rate and is typically  $\mathcal{O}(100)$  (or possibly smaller, depending on the exact time-dependence of thermal effective potential), while  $\epsilon_\star \sim \delta_\star^{-2(-1)} v_w^{3(1)}$  if the signal is sourced by bubble collisions (sound waves), where  $v_w \leq 1$  is the bubble wall velocity (see e.g. [55]). Therefore, achieving such a large GW signal from a PT at a scale not far from 100 MeV requires a large value of  $\alpha_\star$ ,<sup>3</sup> and a mildly efficient damping of the DS energy density into the SM thermal bath before BBN. Such a coupling between the SM and new particles of  $\mathcal{O}(\text{GeV})$  mass could lie in a wide range, as it would not suffer from significant constraints from supernova emission for such masses [109], and could be probed in principle by laboratory experiments.

<sup>3</sup> For PTs,  $\alpha_\star \gtrsim 1$  implies that the PT is supercooled and the Universe undergoes a low-scale inflationary phase. A viable cosmology then requires exiting such a supercooled phase and reheating the Universe above Big Bang Nucleosynthesis, which might be challenging in concrete models, see e.g. [108] for a discussion in a different context. A similar remark applies to the case of domain walls (DWs), although in this case exit from DW domination is likely not possible, thus  $\alpha_\star \leq 1$  should be imposed.

A scenario that can potentially evade the constraints above, while still exhibiting a CT, is that of GWs induced by the collapse of large density fluctuations [66, 110–114]. This can occur if the curvature power spectrum is enhanced at scales  $k \gtrsim 10^6 \text{ Mpc}^{-1}$ , much smaller than those probed by CMB anisotropies [20, 24, 28, 29, 115–122]. However, for the CT to be relevant in the induced GW scenario, the peak of the SGWB should be reached at frequencies higher than those observed with PTA experiments, and with a peak amplitude  $h^2 \Omega_{\text{GW}}(f_\star) \gtrsim 10^{-8}$  (see also [24]). Therefore, the required large scalar perturbation amplitude would generate an unacceptably large relic abundance of PBHs (see e.g. [123, 124] for reviews), unless negative non-Gaussianities suppressing PBH formation are present [125] (overproduction of PBHs in Gaussian models has been shown to significantly constrain the interpretation of the excess already in the IPTA-DR2 and NANOgrav 12.5 years datasets in Ref. [24]). Thus, a viable explanation of the PTA signal by second order GW requires the scalar source to be active around the horizon crossing of nHz modes, with a different specific imprint from the QCD crossover era (see e.g. [62, 126]).

Finally, let us stress that our discussion does not generically apply to sources that are active on time scales much larger than one Hubble time, such as cosmic strings. These sources are not expected to exhibit a CT, and their GW signal is also not characterized by Eqs. (A3) and (C1). However, the interpretation of the PTA excess in terms of strings generated by the spontaneous breaking of a global symmetry (such as arise in axion models, notice that if the axion is massive then the string network disappears once the corresponding domain walls form and the GW signal then features a CT as usual) faces constraints from cosmology, see [127].

*c. Impact of the bound from  $\Delta N_{\text{eff}}$  on the amplitude of  $\Omega_{\text{GW}}(f_\star)$ .* This consistency condition, that only applies to the scenario where the source for GW emission is a cosmological phase transition, becomes relevant when confronted with the requirement of falling below the bound from  $\Delta N_{\text{eff}}$ . Given the amplitude required to explain the PTA signal, by extrapolating the CT we would infer  $f_\star \lesssim 60 \text{ nHz}$ . By accounting for the relation between the peak frequency and the duration of the transition  $\beta^{-1}$ , this would force us to  $\beta/H_\star \lesssim 1.3 \cdot (150 \text{ MeV}/T_\star)$ . On top of this upper bound, there is a lower bound imposed by our assumption about the CT lying around the QCD transition,  $T_\star > T_{\text{QCD}}$ . Given that  $\beta > H_\star$ , these equations would imply  $T_\star \simeq [150, 200] \text{ MeV}$ .

This back-of-the-envelope estimate is, however, overly restrictive for various reasons.

*i)* First, the parameter space for our assumptions to be consistent becomes larger if one considers phase transitions with non-relativistic bubble wall velocities  $v_w < 1$ . Smaller velocities would lead to an additional scaling of the peak frequency that follows  $f_\star \propto 0.35/(1 + 0.07v_w + 0.69v_w^4)$  or  $f_\star = 0.536/v_w$  for the bubble or

sound waves contribution respectively.

*ii)* Secondly, the approximately cubic scaling dictated by causality arguments is expected to break down before the peak frequency, and the SGWB is much less steep between  $f_{\text{CT}}$  and  $f_\star$ . This alleviates the upper bound from  $\Delta N_{\text{eff}}$ . We show this possibility in Fig. 4, where we

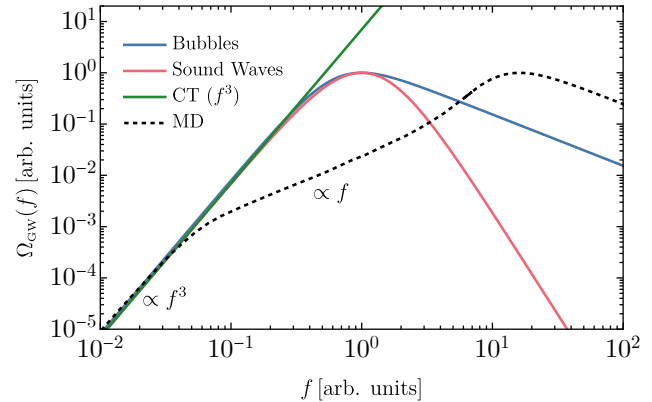


FIG. 4. Spectra of SGWB induced by first order PT. We normalise the frequency in terms of the peak frequency  $f_\star$  while factorise out the overall spectral amplitude. We show both the expected contribution of bubble collisions and sound waves. In green we indicate the causality tail obtained assuming perfect radiation domination, while the black dashed line indicates the effect of an intervening matter domination (MD) phase that would shift the peak to larger frequencies.

adopt the following parametrisation for the contribution of bubble collisions [128]

$$\Omega_{\text{GW}}(f) \propto \frac{(a+b)^c}{[bx^{-a/c} + ax^{b/c}]^c}, \quad (\text{C2})$$

with  $(a, b, c) = (3, 1, 1.5)$  [21] and sound waves [129]

$$\Omega_{\text{GW}}(f) \propto x^3 \left( \frac{7}{4 + 3x^2} \right)^{7/2}. \quad (\text{C3})$$

Here, for simplicity, we are neglecting the effects of the QCD crossover on the CT, as they do not affect this discussion. Due to the breaking of the  $f^3$  scaling close to the peak,  $\Omega_{\text{GW}}$  is lower than the one obtained extrapolating the CT up to peak frequency of a factor  $\mathcal{O}(6)$ .

*iii)* Lastly, an additional model dependence is still possible. In particular, as also discussed in App. D, one may envision an intermediate matter dominated phase that could effectively break the cubic scaling with an intermediate linear growth  $\Omega_{\text{GW}}(f) \propto f$ . As a consequence, depending on the duration of the intermediate matter phase, the bound on the SGWB amplitude in the CT could be relaxed, effectively shifting the onset of the cubic drop-off.

### D. Effects of intermediate matter domination

The interpretation of our results presented in the discussion in the main text are based on Eqs. (A3) and (C1), which assume a standard radiation-dominated (RD) Universe until matter-radiation equality. Changes to the expansion history may have occurred before Big Bang Nucleosynthesis, and would alter the GW relic abundance, as well as the peak frequency and the CT.

The simplest example is arguably that of an early phase of matter domination (MD) when or right after the GW source is active, such as the one that can be due to the slow decay of a massive particle. For the purpose of understanding the effects on the GW signal, we parametrize the duration of the MD phase by the ratio of the initial temperature  $T_i$  at the onset of MD (if it occurs below  $T_*$ , otherwise  $T_i = T_*$ ) and that at the beginning of the subsequent phase of RD,  $r \equiv T_f/T_i < 1$ . As mentioned in Sec. II, the CT can be dramatically altered in this case, and increases with frequency as  $f$ . Notice that the effects of the QCD crossover are in this case washed out, since the SM radiation bath is necessarily a subleading component of the Universe in this scenario.

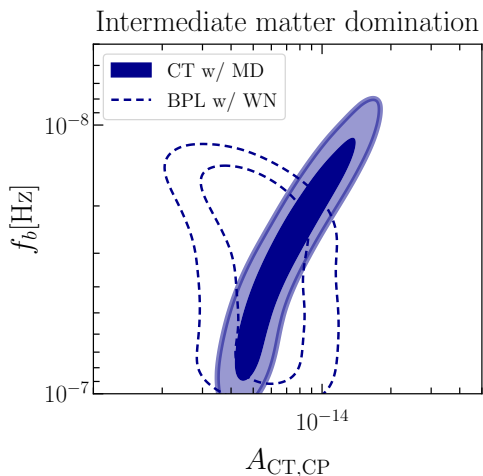


FIG. 5. 2d posteriors of the amplitude of the CT with MD (Broken PL with white noise) and the bending frequency of the signals.

To model the CT in the presence of a transition from a RD era to a matter dominated (MD) era, we use the following broken power-law parametrization for the characteristic strain:

$$h_{c,MD}(f) = A_{CT} \left( \frac{f}{f_{yr}} \right)^{\frac{3-\gamma_{MD}}{2}} \times \left[ 1 + \left( \frac{f}{f_{b,MD}} \right)^{\frac{1}{\kappa_{MD}}} \right]^{\kappa_{MD}-\delta_{MD}}, \quad (D1)$$

with  $\gamma_{MD} = 4$  (low frequency, MD) and  $\delta_{MD} = 2$  (high frequency, RD). The bending frequency  $f_{b,MD}$

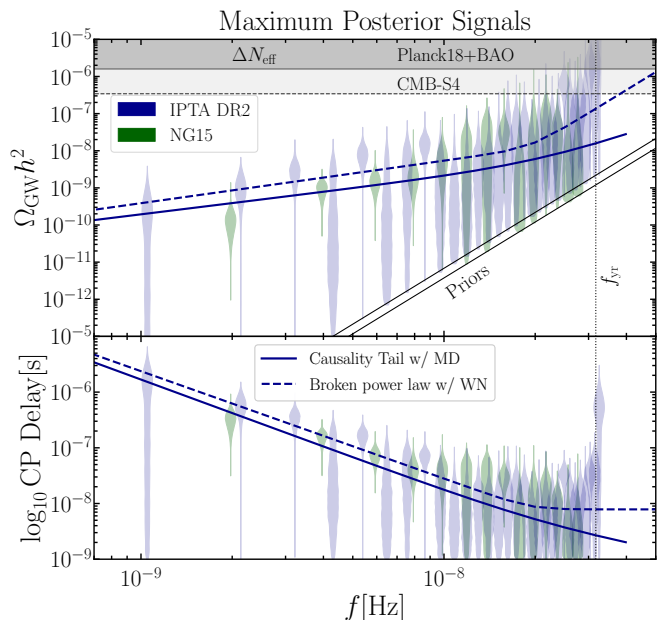


FIG. 6. Similarly to Fig. 2, we show the best fits to IPTA-DR2 data with two different models: in dashed, the broken power law model with white noise at high frequencies, with values of bending frequencies determined by our Bayesian analyses; in solid, the CT signals corresponding to intermediate phase of matter domination. The violin-shaped posteriors are adapted from the results of [11] (IPTA-DR2) and [2] (NG15), with lower limits determined by prior choices as in Fig. 2.

corresponds to the temperature of the transition from radiation to matter domination. The choice  $\kappa_{MD} = 0.4$  reproduces the result of [40] well enough for our purposes.

We performed a Bayesian search for such a MD-altered CT in the IPTA-DR2 dataset. additionally including the effects of free-streaming GWs as in (6) of the main text, see also the discussion in the second paragraph of Sec. IV. To illustrate how this scenario of MD-altered CT signal would compare with data, we show the curves obtained with maximum-posterior values of  $f_{b,MD}$  and  $A_{CT}$  for IPTA-DR2 (this time including all 30 bins) in Fig. 6. For the bending frequency, the value used in Fig. 6 is 25 nHz, corresponding to  $T_i \simeq 800$  MeV. For comparison, we also plot the model-agnostic broken power law with white noise in  $A_{CP}$  at high frequencies, as in the analyses of the IPTA-DR2 collaborations [11] (the curves are obtained by letting the bending frequency, as well as the low-frequency slope and the amplitude free to vary, notice that the difference of our results with respect to those of the collaboration is due to the fact that we are using the maximum posterior values of each parameter, rather than the maximum likelihood signals).

We then compare the models with the choices discussed above. The resulting Bayes factor is  $\log_{10} \mathcal{B}_{CT+MD, BPL} \simeq 1.2$ , showing that a CT signal affected by matter domination below the QCD crossover fits the full IPTA-DR2 30 bins dataset better than a

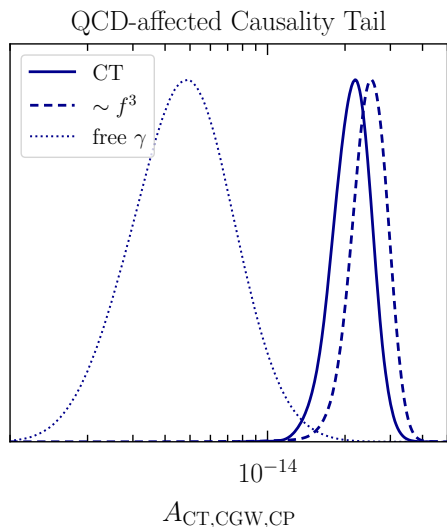


FIG. 7. 1d posteriors of the amplitude of the CT,  $f^3$  and free  $\gamma$  (CP) signals, obtained using the IPTA-DR2 dataset.

broken power law with white noise at high frequencies, although the latter might still be considered as a more motivated model. The 2d posteriors resulting from fitting separately the two models to the data are shown in Fig. 5. We find:  $\log_{10} A_{\text{CT}} = -14.15^{+0.13}_{-0.21}$ ,  $\log_{10} f_{b,\text{MD}} = -7.51^{+0.27}_{-0.34}$  and  $\log_{10} f_{b,\text{MD}} = -7.47^{+0.42}_{-0.35}$ ,  $\gamma_{\text{BPL}} = 3.87 \pm 0.36$ , where the error bars denote the 68% C.L. ranges.

Following the above considerations, it is important to notice that additional suppression factors in both the peak frequency (A3),  $\sim r^{1/3}$ , and amplitude in (C1),  $r^{4/3}$  (if the source is active during MD) arise. Requiring the CT to be in the first bins of the PTA sensitivity band implies that its amplitude is  $O(10^{-7} - 10^{-8})$  at  $f_{\text{yr}}$ . In turn, this requires  $\alpha \gtrsim (0.1 - 0.3)r^{-2/3}$ . On the other hand, successful BBN imposes  $T_f \gtrsim 5 \text{ MeV}$ , i.e.  $r \gtrsim 0.005$  for  $f_* \simeq 10^{-7} \text{ Hz}$ , with the inequality becoming weaker (stronger) if  $f_*$  is larger (smaller). Therefore the GW source could have overcome the radiation background, if

the MD phase lasted until temperatures corresponding to the first frequency bins of PTA datasets.

### E. Details of the numerical analysis and additional posteriors

Here we report details of our numerical analysis. We have performed it using the codes `enterprise` [95] and `enterprise_extensions` [96], in which we implemented the CT signal reported in Fig. 1, and use PTMCMC [97] to obtain MonteCarlo samples. We derive posterior distributions using `GetDist` [130]. We include noise parameters (white, red and dispersion measure) according to the strategy of the IPTA DR2 [11] collaboration. For more details, see also the Appendix of [23].

Our prior choices for noise and GW parameters are reported in Table III. In order to produce the results reported in the main text, we have restricted our analyses to the first 13 frequency bins of the IPTA-DR2 datasets respectively, as in [11]. We obtained more than  $10^6$  (typically  $5 \cdot 10^6$ ) samples per each analysis and model in this work, and discarded the first 25% of each chain. With these choices, we reproduce the posteriors for CP parameters presented in [11] with excellent agreement.

The upper prior boundary on the amplitude of cosmological signals is set by the  $\Delta N_{\text{eff}}$  bound reported in Eq. (7), setting  $f_{\text{CT}} = f_{\text{yr}}$  for the analyses reported in the main text to set ideas.

We employed all 30 frequency bins of the IPTA-DR2 datasets for the intermediate MD analysis presented in App. D.

We show the 1d posteriors for the amplitude of the GW signals considered in Sec. IV of the main text in Fig. 7. We find:  $\log_{10} A_{\text{CT}} = -13.67^{+0.08}_{-0.07}$ ,  $\log_{10} A_{f^3} = -13.61^{+0.08}_{-0.06}$  and  $\log_{10} A_{\text{CP}} = -14.33 \pm 0.2$ ,  $\gamma = 3.94 \pm 0.44$  for the CP signal with free  $\gamma$ , where the error bars denote the 68% C.L. ranges.

<i>Parameter</i>	<i>Description</i>	<i>Prior</i>	<i>Comments</i>
<b>White Noise</b>			
$E_k$	EFAC per backend/receiver system	Uniform [0, 10]	single-pulsar only
$Q_k[s]$	EQUAD per backend/receiver system	log-Uniform [-8.5, -5]	single-pulsar only
$J_k[s]$	ECORR per backend/receiver system	log-Uniform [-8.5, -5]	single-pulsar only (NG9)
<b>Red Noise</b>			
$A_{\text{red}}$	Red noise power-law amplitude	log-Uniform [-20, -11]	one parameter per pulsar
$\gamma_{\text{red}}$	Red noise power-law spectral index	Uniform [0, 7]	one parameter per pulsar
<b>DM Variations Gaussian Process Noise</b>			
$A_{\text{DM}}$	DM noise power-law amplitude	log-Uniform [-20, -11]	one parameter per pulsar
$\gamma_{\text{DM}}$	DM noise power-law spectral index	Uniform [0, 7]	one parameter per pulsar
<b>Causality Tail</b>			
$A_{\text{CT}}$	Strain amplitude at $f = f_{\text{yr}}$	log-Uniform [-18, set by Eq. (7)]	one parameter per PTA
<b><math>f^3</math></b>			
$A_{\text{CGW}}$	Strain amplitude at $f = f_{\text{yr}}$	log-Uniform [-18, set by Eq. (7)]	one parameter per PTA
<b>Supermassive Black Hole Binaries (SMBHBs)</b>			
$A_{\text{SMBHB}}$	Strain amplitude at $f = f_{\text{yr}}$	log-Uniform [-18, -11]	one parameter per PTA
<b>Power law</b>			
$A_{\text{GWB}}$	Strain amplitude at $f = f_{\text{yr}}$	log-Uniform [-18, -13]	one parameter per PTA
$\gamma_{\text{GWB}}$	GWB power-law spectral index	Uniform [0, 7]	one parameter per PTA
<b>Matter domination CT</b>			
$A_{\text{CT}}$	Strain amplitude at $f = f_{\text{yr}}$	log-Uniform [-18, -11]	one parameter per PTA
$\gamma_{\text{MD}}$	CT low frequency power-law spectral index	Fixed to 4	one parameter per PTA
$\delta_{\text{MD}}$	CT high-frequency power-law spectral index	Fixed to 2	one parameter per PTA
$f_{b,\text{MD}}$	CT bending frequency (MD to RD transition)	log-Uniform [-10, -7]	one parameter for PTA
$\kappa_{\text{MD}}$	Width of matter to radiation transition	Fixed to 0.4	one parameter per PTA
<b>High frequency noise Broken power law</b>			
$A_{\text{GWB}}$	Strain amplitude at $f = f_{\text{yr}}$	log-Uniform [-18, -11]	one parameter per PTA
$\gamma_{\text{GWB}}$	GWB low frequency power-law spectral index	Uniform [0, 7]	one parameter per PTA
$\delta_{\text{GWB}}$	CT high-frequency power-law spectral index	Fixed to 0	one parameter per PTA
$f_b$	GWB bending frequency (signal to noise transition)	log-Uniform [-10, -7]	one parameter per PTA
$\kappa_{\text{GWB}}$	Width of signal to noise transition	Fixed to: 0.1	one parameter per PTA

TABLE III. List of noise and GWB parameters used in our analyses, together with their prior ranges.